

Article

Activated Sintering of Cr₂O₃-Based Composites by Hot Pressing

Edwin Gevorkyan ^{1,2}, Lenka Cepova ³, Mirosław Rucki ^{2,*}, Volodymyr Nerubatskyi ¹,
Dmitrij Morozow ⁴, Wojciech Zurowski ⁴, Voskan Barsamyan ⁵ and Karel Kouril ⁶

- ¹ Faculty of Mechanical and Energy, Ukrainian State University of Railway Transport, 7 Feuerbach Sq., 61050 Kharkiv, Ukraine
- ² Institute of Mechanical Science, Vilnius Gediminas Technical University, J. Basanaviciaus Str. 28, LT-03224 Vilnius, Lithuania
- ³ Faculty of Mechanical Engineering, VSB-Technical University of Ostrava, 17. listopadu 2172/15, 70800 Ostrava Poruba, Czech Republic
- ⁴ Faculty of Mechanical Engineering, Kazimierz Pulaski University of Technology and Humanities in Radom, Stasieckiego 54, 26-600 Radom, Poland
- ⁵ National Polytechnic University of Armenia, Vanadzor 2011, Armenia
- ⁶ Faculty of Mechanical Engineering, Brno University of Technology, Technicka 2896/2, 61669 Brno, Czech Republic
- * Correspondence: m.rucki@uthrad.pl

Abstract: The paper presents and discusses questions on structure formation during the sintering process of Cr₂O₃-based composites using the hot pressing method, when a chemical reaction between the components takes place. The task was difficult because Cr₂O₃ decomposes when sintered at temperatures above 1300 °C. The proposed novel method allowed for interaction between aluminum and chromia, thus avoiding the decomposition of the latter. Here, ultrafine aluminum powder played the role of the active agent forming a liquid phase and reacting with Cr₂O₃. The appearance of the solid solutions of (Cr,Al)₂O₃ with different stoichiometry of Cr and Al depended on the aluminum content in the initial mixture. The solid solution significantly strengthened boundaries between composite phases, resulting in the composite material of high fracture toughness between 5 and 7 MPa m^{1/2} and bending strength of ca. 500 MPa. The best mechanical properties exhibited the cermet with 22 wt.% of the restored chromium.

Keywords: composite; chromium oxide; reactive sintering; solid solution; phase boundaries



Citation: Gevorkyan, E.; Cepova, L.; Rucki, M.; Nerubatskyi, V.; Morozow, D.; Zurowski, W.; Barsamyan, V.; Kouril, K. Activated Sintering of Cr₂O₃-Based Composites by Hot Pressing. *Materials* **2022**, *15*, 5960. <https://doi.org/10.3390/ma15175960>

Academic Editor: Dina Dudina

Received: 18 July 2022

Accepted: 26 August 2022

Published: 29 August 2022

Publisher's Note: MDPI stays neutral with regard to jurisdictional claims in published maps and institutional affiliations.



Copyright: © 2022 by the authors. Licensee MDPI, Basel, Switzerland. This article is an open access article distributed under the terms and conditions of the Creative Commons Attribution (CC BY) license (<https://creativecommons.org/licenses/by/4.0/>).

1. Introduction

Metal oxides are very important for the composite industry. In ceramic matrix composites, they form the matrix phase, providing high thermal and chemical stability, high compressive strength, high elastic modulus and other advantageous properties [1].

Alumina-based ceramics are popular materials for cutting tools due to their good wear resistance, high hardness, heat resistance and chemical stability [2]. There are many reports on the effects of various reinforcements, such as graphene [3], SiC [4,5], SiC_w-Si₃N₄ [6], TiC [7], TiC-TiN [8] and WC [9], and the works on property improvement are still going on. Basically, sintering methods are used for the fabrication of ceramic matrix composites [10–12]. Recently, the addition of amorphous phases was found useful for preparing micro/nano bimodal microstructures [13].

Compared to aluminum oxide (Al₂O₃), chromia has higher hardness and melting temperature, so ceramic composites based on chromium oxide (Cr₂O₃) can be expected to be advantageous for cutting tool applications. It was initially demonstrated that these composites provided a high quality of the machined hard steel surfaces [14]. The application of chromium oxide based composites for the machining of high-hardness steels seems to be advantageous compared to the traditional, non-regrindable cutting inserts made from aluminum oxide (Al₂O₃) and silicon nitride (Si₃N₄). Especially beneficial is the increase in

machined surface quality, which in some conditions even provides accuracy after reaching close to that obtained after grinding. However, chromia is rather added to the alumina composites to enhance their properties [15], with rare attempts to sinter a Cr_2O_3 -based composite. This is because of the difficulties in obtaining sintered chromia-based dense composite due to the decomposition of Cr_2O_3 at temperatures above $1300\text{ }^\circ\text{C}$.

Cr_2O_3 is a hexagonal crystal with a melting point of $2435\text{ }^\circ\text{C}$ and a high Vicker's hardness of 1825 HV [16]. Chromium oxide (Cr_2O_3) is widely known as a catalyst [17], but it also exhibits high abrasive properties and thus has been widely used in form of polishing pastes. It is an important refractory material with high melting temperature and high oxidation resistance at elevated temperature [18]. Chromia coatings have been widely applied for wear- and corrosion-resistant components in different sectors of industry [19]. Moreover, chromia coatings exhibit high mechanical strength and high microhardness [20]. Since most of the mechanical characteristics of chromia are better than those of alumina, a Cr_2O_3 -based composite for cutting tools can be expected to be advantageous, if it would be possible to avoid the decomposition of chromia during sintering.

The addition of chromia to alumina provides the alumina–chromia solid solutions that are widely used in many applications where high-temperature corrosion resistance is required [21]. From the perspective of cutting tool requirements, a composite Cr_2O_3 –22 wt.% Cr is the most interesting, due to the appearance of eutectics of finely dispersed structure [22]. In this structure, small spherical chromium reinforcement particles are distributed within the Cr_2O_3 matrix.

The present study is devoted to the sintering of a chromia-based composite with an aluminothermic reaction, where the metallic chromium is released. The objective is to calculate the respective proportion of the initial components leading to a proper eutectic composition after sintering that results in advantageous properties of the sintered Cr_2O_3 -based composite.

2. Materials and Methods

Initial powders used for the experiments were finely crushed, ultradispersed ones. Cr_2O_3 powder delivered by Sigma Aldrich Chemie GmbH (Taufkirchen, Germany) had particle dimensions between 1 and $3\text{ }\mu\text{m}$, while the aluminum powder type PAP-2, made by PromMetal (Moscow, Russia), had particles in form of small plates from several microns to $30\text{ }\mu\text{m}$ large. The SEM images of the powders are shown in Figure 1.

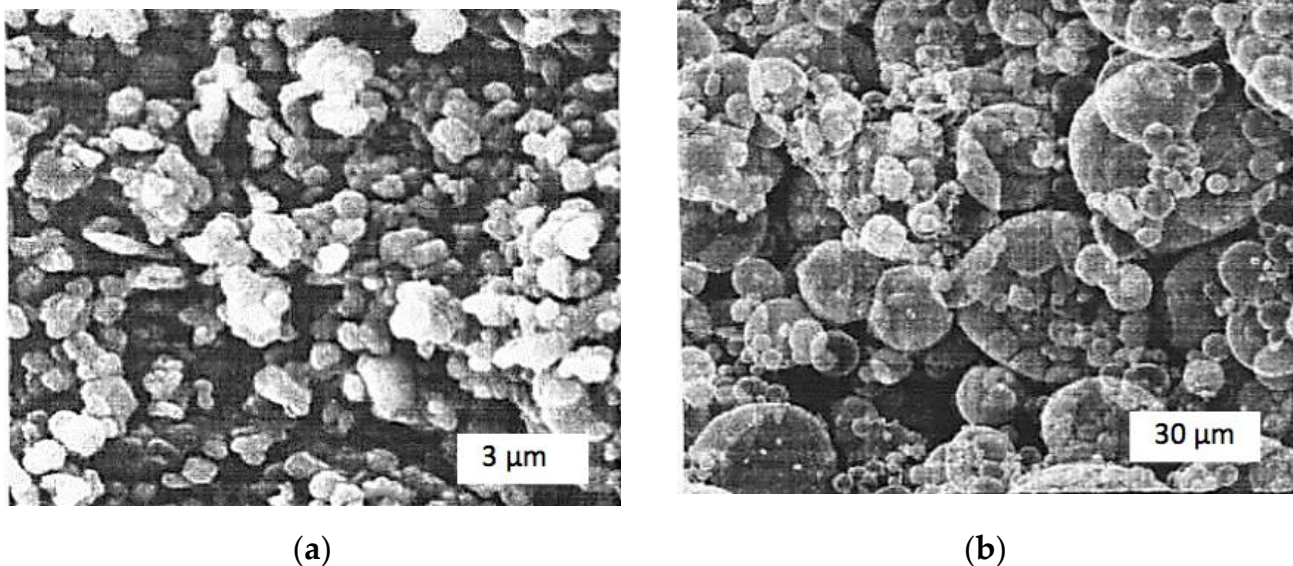


Figure 1. SEM images of the initial powders: (a) Cr_2O_3 ; (b) Al.

The powders were mixed together in the agate drums using a planetary ball mill, at a speed of 5 m/s for 30 min in the environment of ethanol. The proportion of the powder mixture, ethanol and mixing balls was 2:1:1. After the procedure, the mixtures were dried and rubbed through a #0064 sieve.

The powder mixture of chromium oxide and aluminum was then briquetted in steel molds in a vacuum. These samples then underwent a hot pressing procedure in a vacuum of 10^{-2} Pa under a pressure of 30 MPa in the electric field.

In order to investigate the interaction between the powders of Cr_2O_3 and aluminum in the mixture, differential thermal analysis (DTA) was employed. In the original device, a patented high-temperature unit was installed, enabling analysis of the thermal effects of chemical reactions [23]. For that purpose, a powder mixture of $\text{Cr}_2\text{O}_3 + 13$ wt.% Al was prepared.

The physical and mechanical characteristics of the tested composites were determined with standard methodology and devices. The flexural strength was measured using an MH-1 machine with samples of dimensions $5 \times 5 \times 35$, base 30 mm. Concentrated force was applied at a velocity of 40 m/s, and in one pack, there were 5 samples.

Compressive strength was measured using the standard device UMN-10 produced by Alexandrov Factory (Alexandrovka, Russia). The respective samples were ground until the methodologically recommended parameters [24] were reached. Five samples of dimensions $5 \times 5 \times 10$ mm were used for one point. The Microhardness of the composites was measured using a PMT 3 GEO-NDT device (Russia) with optimal loads and time of measurement.

The fracture toughness K_{IC} was determined from the indentation with Vickers' pyramid on the polished surfaces according to the following formula [25,26]:

$$K_{IC} \cdot F \left(H \cdot a^{\frac{1}{2}} \right) \cdot \left(\frac{H}{E \cdot F} \right)^{\frac{2}{5}} = 0.35 \cdot \left(\frac{l}{a} \right)^{-\frac{1}{2}}, \quad (1)$$

where F is the constraint factor, $F = 3$; H is the hardness; a is the half-diagonal of the Vickers indent; E is the Young's modulus; and l is the length of the surface crack. The dimensions of samples made for that purpose were $13 \text{ mm} \times 13 \text{ mm} \times 5 \text{ mm}$.

Relative density D_r was calculated using the following equation:

$$D_r = \frac{D_b}{D_{th}} \cdot 100\%, \quad (2)$$

where D_b is the actual density of a sintered specimen in g/cm^3 and D_{th} is the theoretical density of the solid material in g/cm^3 .

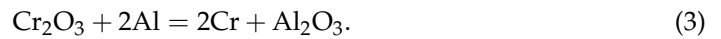
XRD spectra of the powders were measured using Dron-3.0 and URS-50 diffractometers with $\text{Cu-K}\alpha$ radiation and Ni filter.

A fractography study was carried out using a scanning electron microscope (SEM) JEOL JSM-840 (JEOL, Tokyo, Japan). Micro XRD analysis was performed with a Cam-Scan series SEM, which enabled the assessment of the qualitative, semi-quantitative and quantitative distribution of the components on the surface points. Qualitative chemical analysis along the profile was performed with the Link-860 energy-dispersive spectroscopy (EDS) system (Link Systems Ltd., High Wycombe, UK), while the ZAF-4 correction factor was used for the quantitative determination of chemical composition. Semi-quantitative assessment was performed using Digimap proprietary software. All the results underwent statistical analysis.

A metallographic study of the obtained structures was performed using the MIM-8 (LOMO, St. Petersburg, Russia) microscope in reflected light, with a zoom from $300\times$ to $1000\times$. For that purpose, the samples were ground with diamond discs of 60/40, 20/14, 7/5 and $3/2 \mu\text{m}$ grains with a coolant in form of water emulsion.

3. Theoretical Background

According to the main goal of the research, it is crucial to determine the initial proportion of powders in order to find the final proportion of components preventing the decomposition of chromia. It is known that in the composite structure, chromium can be obtained from the chromium oxide through the aluminothermic reaction [27]:



From this equation, it is seen that by varying the aluminum content in the initial powder, it is possible to fabricate composite materials of different compositions and stoichiometry and thus with different properties. Among other materials, it is possible to obtain the abovementioned eutectic composition indicated in [22] (see Section 1). A simple assessment indicates that the target 22 wt.% chromium will be restored when the initial chromia powder contains 13 wt.% aluminum. When processing the powder mixture of $\text{Cr}_2\text{O}_3 + 13 \text{ wt.}\% \text{ Al}$, it was expected to obtain the final products of reaction with the required eutectic proportion of chromium: $\text{Cr}_2\text{O}_3 + (\text{Cr,Al})_2 + 22 \text{ wt.}\% \text{ Cr}$.

It is a known fact that the effectiveness of this process is dependent on the particle dimensions of both metal oxide and aluminum, as well as on the mixture composition. Apparently, the finer the powder is, the more intense the reaction is.

4. Results and Discussion

4.1. Effect of Sintering Conditions on Relative Density

The DTA curve shown in Figure 2 demonstrated that the interaction between chromium oxide and aluminum started at 825 °C. A substantial exothermal effect took place at 895 °C, while the presence of the exothermal effect at 660 °C was related to the initiation of the aluminum powder melting process.

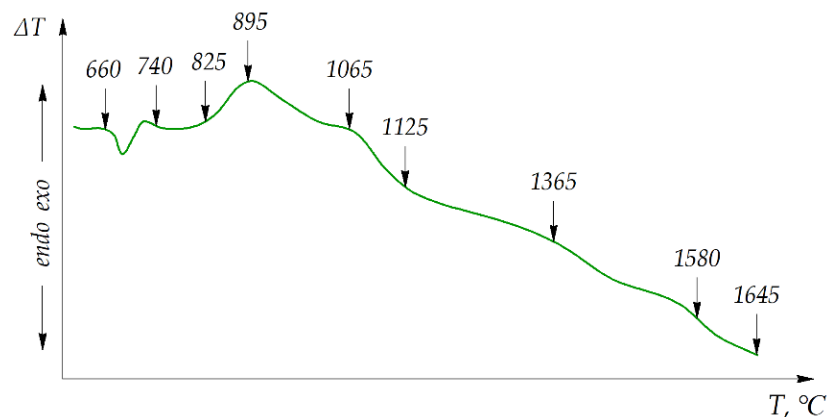


Figure 2. Thermogram of the initial powder mixture $\text{Cr}_2\text{O}_3 + 13 \text{ wt.}\% \text{ Al}$.

Thermal equilibrium can be described by the following equation [28]:

$$\alpha \cdot (T_a - T_s) = m_s \cdot C \cdot n_s \cdot V + q \cdot \left(\frac{dm_s}{dt} \right) + m_0 + C_0 \cdot V + q_{loss}, \quad (4)$$

where α is the coefficient of proportion, T is temperature, m is mass, C is specific heat capacity, q is specific enthalpy of transformation and q_{loss} is heat loss; a —ambient, s —sample, o —outer surface.

When the aluminum content in the mixture was 13 wt.%, the specific heat released during the reaction was $Q = 925 \text{ J/kg}$. It was found that heat release for the mixtures with lower aluminum amounts was smaller; e.g., the mixture $\text{Cr}_2\text{O}_3 + 13 \text{ wt.}\% \text{ Al}$ provided $Q = 712 \text{ J/kg}$. Hence, the sintering temperature for a higher Al proportion is higher.

Equilibrium parameters for the thermodynamical system were found from the determined extrema of the system's entropy. Equilibrium concentration C_e of the components for

the cermet sintered from the mixture $\text{Cr}_2\text{O}_3 + 13 \text{ wt.}\% \text{ Al}$ was calculated for the temperature T range from $700 \text{ }^\circ\text{C}$ to $1400 \text{ }^\circ\text{C}$ and the pressure P range from 30 MPa to 0.01 MPa . The results of the calculations are shown in Table 1.

Table 1. Calculated equilibrium concentration C_e in mol/L of components in the cermet obtained by hot pressing of powders $\text{Cr}_2\text{O}_3 + 13 \text{ wt.}\% \text{ Al}$ under different pressure P and temperature T conditions.

$T, \text{ }^\circ\text{C}$	Components	$P = 30 \text{ MPa}$	$P = 0.1 \text{ MPa}$	$P = 0.01 \text{ MPa}$
700	Cr_2O_3	1.217	1.055	1.055
	Al_2O_3	3.917	0.407	4.077
	Cr	7.835	8.153	8.158
	Al	0.001	–	–
800	Cr_2O_3	2.385	1.055	0.087
	Al_2O_3	0.052	4.077	4.843
	Cr	8.104	8.153	9.687
	Al	0.049	–	–
900	Cr_2O_3	1.055	1.055	1.055
	Al_2O_3	4.077	4.077	4.077
	Cr	8.153	8.153	8.153
	Al	–	–	–
1000	Cr_2O_3	1.055	1.055	1.055
	Al_2O_3	4.077	4.077	4.077
	Cr	8.153	8.153	8.158
	Al	–	–	–
1100	Cr_2O_3	0.721	0.621	0.621
	Al_2O_3	1.368	0.319	0.319
	Cr	4.346	6.214	6.214
	Al	1.030	–	–
1200	Cr_2O_3	0.965	0.621	0.621
	Al_2O_3	1.063	0.319	0.319
	Cr	5.605	6.214	6.214
	Al	0.065	–	–
1300	Cr_2O_3	1.217	0.422	0.422
	Al_2O_3	0.698	0.915	0.915
	Cr	6.713	7.215	7.215
	Al	–	–	–
1400	Cr_2O_3	1.217	0.422	0.422
	Al_2O_3	0.698	0.915	0.915
	Cr	6.713	7.215	7.215
	Al	–	–	–

From Table 1 it can be seen that under pressure $P = 30 \text{ MPa}$, the increased temperature caused variations in the concentrations of the components; in particular, chromium concentration increased while Cr_2O_3 and Al concentrations decreased. When the pressure was very low, $P = 0.01 \text{ MPa}$, chromium content also increased with the increase in temperature, while aluminum practically disappeared. However, the calculated equilibrium concentration did not change substantially in the temperatures around $900\text{--}1000 \text{ }^\circ\text{C}$ and $1000\text{--}1400 \text{ }^\circ\text{C}$ at the pressure $P = 30 \text{ MPa}$.

Hence, the calculations suggested that the sintering in temperature interval between $1300 \text{ }^\circ\text{C}$ and $1400 \text{ }^\circ\text{C}$ under the pressure of 30 MPa would result in no aluminum among the final products. Thus, these conditions ensure that the restoration reaction is fully completed. Moreover, it is possible to control, to some extent, the composition of the sintered sample with alteration of temperature and pressure.

It should be noted that other processes such as viscous flow and diffusion take place during hot pressing. Figure 3 demonstrates that at $T = 1600 \text{ }^\circ\text{C}$, almost full density can be reached after 2 and 4 min under pressure $P = 30 \text{ MPa}$ and 22 MPa , respectively. Intense

compaction can be attributed to the appearance of the liquid phase of molten aluminum above 660 °C, as well as exothermal reaction temperature increase at 895 °C.

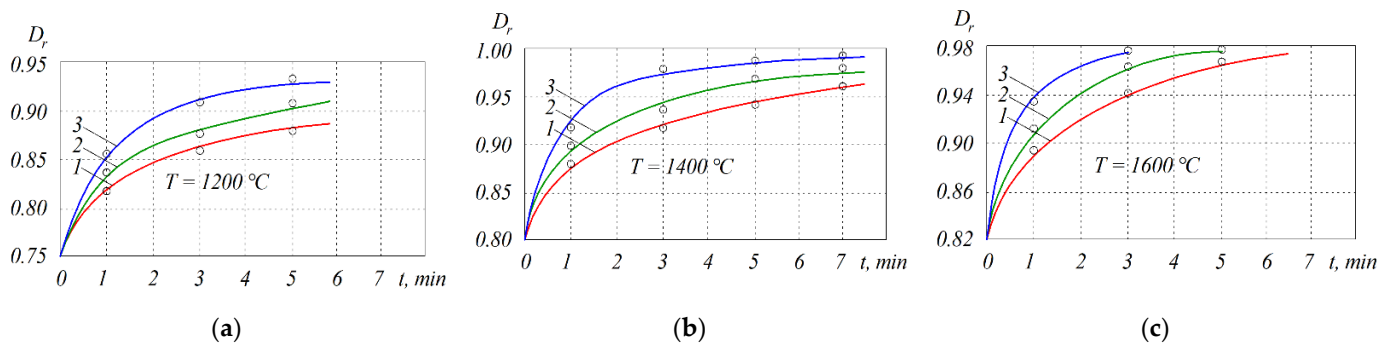


Figure 3. Interpolated curves of relative density D_r of the $\text{Cr}_2\text{O}_3 + (\text{Cr,Al})_2\text{O}_3 + 22 \text{ wt.}\% \text{ Cr}$ cermets sintered at different temperatures: (a) $T = 1200 \text{ }^\circ\text{C}$; (b) $T = 1400 \text{ }^\circ\text{C}$; (c) $T = 1600 \text{ }^\circ\text{C}$. Plots are denoted as follows: 1— $P = 15 \text{ MPa}$; 2— $P = 22 \text{ MPa}$; 3— $P = 30 \text{ MPa}$.

In the experiments, the heating rate was ca. $400 \text{ }^\circ\text{C}/\text{min}$. The pressure was applied gradually, dependent on the temperature of the graphite molds. After $T = 660 \text{ }^\circ\text{C}$ was reached, the pressure was increased to the maximal value set for the particular experiment. This way the liquid aluminum was distributed steadily in the volume of the sintered cermet.

It should be noted that the densification rate slowed down. This can be attributed to the increase in the volume viscosity of the porous body and subsequent slowing down of the volume deformation rate.

4.2. Effect of Solid Solution

XRD analysis revealed the presence of a solid solution of $(\text{Cr,Al})_2\text{O}_3^*$ in the sintered samples, apart from Cr_2O_3 and restored Cr. Results of the measurements of lattice parameters for different proportions of aluminum in the initial powders are shown in Table 2.

Table 2. Lattice parameters a and c for the sintered powders with different aluminum contents.

No.	Initial Powder Content	$a_1, \text{ \AA}$	$a_2, \text{ \AA}$	$a_3, \text{ \AA}$	$c_1, \text{ \AA}$	$c_2, \text{ \AA}$	$c_3, \text{ \AA}$
1	$\text{Cr}_2\text{O}_3 + 9 \text{ wt.}\% \text{ Al}$	4.947	4.936	4.922	13.302	13.366	13.433
2	$\text{Cr}_2\text{O}_3 + 13 \text{ wt.}\% \text{ Al}$	4.941	4.936	4.922	13.366	13.410	13.433
3	$\text{Cr}_2\text{O}_3 + 17 \text{ wt.}\% \text{ Al}$	4.936	4.926	4.922	13.410	13.428	13.433

These results are in conformity with those of [29], which indicated the appearance of a solid solution between Cr_2O_3 and Al_2O_3 in a certain range of temperature. Oxides of chromium and aluminum have a corundum structure, where ions of oxygen are almost densely packed with ions of Al^{3+} or Cr^{3+} . These occupy two-thirds of the available octahedral positions; thus, the obtained solid solution can be described as $\text{Al}_{2-x}\text{Cr}_x\text{O}_3$ ($0 \leq x \leq 2$). For the in-between values of x , Al^{3+} and Cr^{3+} ions are distributed in octahedral positions disorderly. In a single octahedral cluster, ions of Al^{3+} and Cr^{3+} can be found, and the probability of a particular ion's presence depends on the parameter x .

4.3. Composition of the Obtained Cermets

Results of qualitative analysis of component distribution at the phase boundaries indicate the presence of some sort of transitional layer ca. $2 \text{ }\mu\text{m}$ thick. Figure 4a presents a plot for the $\text{Cr}_2\text{O}_3 + (\text{Cr,Al})_2\text{O}_3 + 22 \text{ wt.}\% \text{ Cr}$ composite made along the line marked LS in Figure 4b, across the grain. The sample was sintered at $T = 1400 \text{ }^\circ\text{C}$ and $P = 30 \text{ MPa}$ for $t = 10 \text{ min}$.

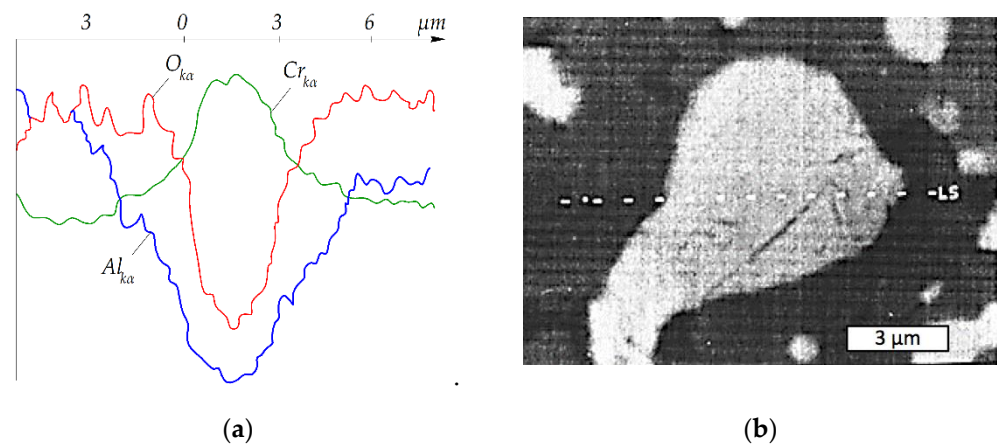


Figure 4. Qualitative distribution of the elements at the phase boundaries in the $\text{Cr}_2\text{O}_3 + (\text{Cr},\text{Al})_2\text{O}_3 + 22 \text{ wt.}\% \text{ Cr}$ sample sintered out of $\text{Cr}_2\text{O}_3 + 13 \text{ wt.}\% \text{ Al}$ powder at $T = 1400 \text{ }^\circ\text{C}$ and $P = 30 \text{ MPa}$ for $t = 10 \text{ min}$: (a) diagram; (b) SEM image of the analyzed sample.

The distribution of elements in the boundary between the ceramic and metal compounds of the composite and the existence of a single phase of ceramic near the metal suggest that the transition zone consists of solid solution $\text{Al}_{2-x}\text{Cr}_x\text{O}_3$. Both literature [29] data and XRD analysis confirmed this assumption. The presence of pure chromium in the gray grain confirmed its full recovery from Cr_2O_3 , according to the expectations and objectives of the experiments.

Moreover, results of the quantitative chemical analysis suggested that the composition of $\text{Al}_{2-x}\text{Cr}_x\text{O}_3$ solid solution depended not only on the aluminum amount, but also on the temperature of hot pressing and on the exposure time t . Table 3 presents the content of chromium and aluminum in the sintered samples of $\text{Cr}_2\text{O}_3 + (\text{Cr},\text{Al})_2\text{O}_3 + 22 \text{ wt.}\% \text{ Cr}$, where the initial composition of powders $\text{Cr}_2\text{O}_3 + 13 \text{ wt.}\% \text{ Al}$ was the same but sintering time t was different.

Table 3. Percentage by weight of Al and Cr in the samples of $\text{Cr}_2\text{O}_3 + (\text{Cr},\text{Al})_2\text{O}_3 + 22 \text{ wt.}\% \text{ Cr}$ sintered at $T = 1400 \text{ }^\circ\text{C}$ and $P = 30 \text{ MPa}$ for different lengths of sintering time t .

Compound	$t = 5 \text{ min}$	$t = 10 \text{ min}$	$t = 15 \text{ min}$
Aluminum	40.5	27	13.5
Chromium	26	52	78

Further XRD analysis revealed that the oxide lattice was substantially deformed. Namely, it formed a Cr_2O_3 structure of rhombohedral space group R3c with coherent addition of complex $(\text{Cr},\text{Al})_2\text{O}_3$ of hereditary structure. From Table 2 above, it can be seen that the aluminum content percentage in the initial powder did not affect the lattice parameters a_3 and c_3 . From this fact, it can be concluded that these parameters are related to the chromium oxide lattice.

However, XRD showed that in the solid solution made out of the same composition, the lattice parameters a_1 , a_3 , c_1 and c_3 are varying for different sintering times. These variations perhaps can be attributed to the concentration of the ions Cr^{3+} and Al^{3+} , which causes a difference between two micro areas rich in aluminum oxide and chromium oxide, respectively. Despite that, macroscopic analysis suggests the homogeneous structure of the solid solution. As a result, there are two different lattice structures with different parameters in the same solid solution. When the proportion of the components in the powder mixture is changed, the lattice parameters change too. In fact, an increase in Al proportion caused a decrease in the a parameter and an increase in the c parameter. Since the ratio c/a increases, the electron structure changes.

Figure 5 shows the plots of chromium, aluminum and oxygen content in the sintered samples of $\text{Cr}_2\text{O}_3 + (\text{Cr,Al})_2\text{O}_3 + 22 \text{ wt.}\% \text{ Cr}$ after different sintering times. It is clear that the proportion of chromium increased for longer sintering times, while that of aluminum decreased, which led to the variation in the composition of the solid solution. The experimental results suggest that the interaction of both oxides at the boundaries between the phases of oxide and metal provides a solid solution of $\text{Al}_{2-x}\text{Cr}_x\text{O}_3$ ($0 \leq x \leq 2$) of varying composition. The quantitative proportion of the compounds in this solution depends on the initial powder composition, as well as on the sintering conditions, above all the temperature and sintering time.

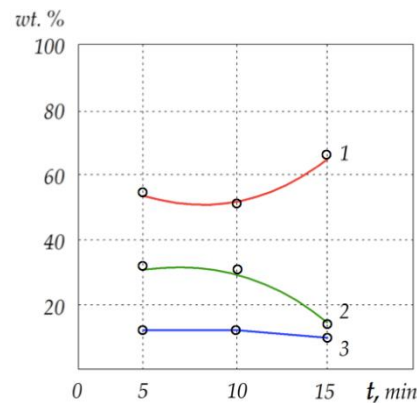


Figure 5. Percentage by weight of components in the dark phase of $\text{Cr}_2\text{O}_3 + (\text{Cr,Al})_2\text{O}_3 + 22 \text{ wt.}\% \text{ Cr}$ cermet samples sintered at $T = 1300 \text{ }^\circ\text{C}$ under $P = 30 \text{ MPA}$ for different lengths of time t . The curves are marked as follows: 1—chromium; 2—aluminum; 3—oxygen.

4.4. Strength Analysis

It is widely known that the strength of MeO–Me cermets is determined by its weakest element, namely the bond of the ceramic/metal interface [30]. The solid solution $\text{Al}_{2-x}\text{Cr}_x\text{O}_3$ resulting from an aluminothermic reaction seems to be the weakest point of the tested composite since it represents an intermediate phase and determines the strength of metal–oxide contact. The simplified scheme of the contact area between the metal (1) and oxide (2) is presented in Figure 6a, and the presence of the transitional phase in presented Figure 6b. An increase in the composite strength is possible when

$$U_{1-2} < U_2; U_{1-2} < U_3; U_{1-2} < U_{1-3}, \quad (5)$$

where U_1 , U_2 and U_3 denote the strengths of metal, oxide and transitional phases, respectively, while U_{1-2} , U_{1-3} and U_{2-3} denote the strengths of the boundaries between the phases [27].

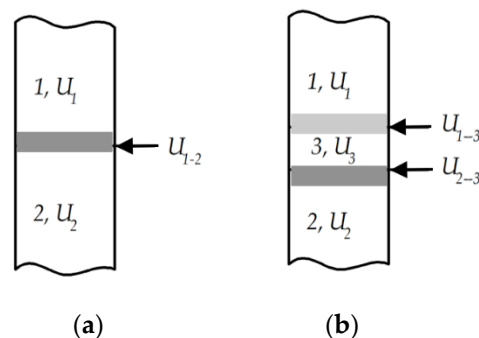


Figure 6. The simplified scheme of contact areas: (a) contact area directly between the metal (1) of strength U_1 and oxide (2) of strength U_2 ; (b) presence of the transitional phase (3) of strength U_3 between the metal (1) and oxide (2).

From the literature, it can be found that chromium oxide is more active than oxides Al_2O_3 and ZrO_2 in interaction with metals [31]. This can be attributed to the basic properties of the metal oxides [32], since the thermodynamic stability of Cr_2O_3 is lower than that of Al_2O_3 and ZrO_2 , while the pressure of its dissociation products is higher than that of Al_2O_3 and ZrO_2 .

During the hot pressing, aluminum melts at the temperature of $660\text{ }^\circ\text{C}$, introducing a liquid phase to the sintered powders. A liquid phase usually serves as a sintering aid for the ceramic matrix composite [33]. The structure and, hence, the mechanical properties of the sintered cermet depend largely on the distribution of the aluminum throughout the sample volume. The molten aluminum wets the solid surface of chromium oxide and starts to interact with it at $825\text{ }^\circ\text{C}$.

Work of adhesion W_a can be calculated from the known equation [34]:

$$W_a = \gamma_A + \gamma_B - \gamma_{AB}, \quad (6)$$

where γ_A and γ_B are the surface energies of the two substances being bonded and γ_{AB} is interfacial energy between phases A and B.

Moreover, since van der Waals forces are in the nanometer range, they are responsible for contact interactions [35], which can be included in the following equation:

$$W_a = W_b + W_{ch}, \quad (7)$$

where W_b is van der Waals interaction energy and W_{ch} is the energy of chemical interaction.

The equilibrium of liquid aluminum on the solid surface of chromium oxide can be described by the so-called Young equation [36]:

$$\frac{(\gamma_{tg} - \gamma_{tz})}{\gamma_{tz}} = \cos \theta, \quad (8)$$

where θ is the equilibrium contact angle and γ is the interfacial free energy; t —solid phase, g —gaseous phase, z —liquid phase.

The equilibrium of liquid aluminum on the solid surface of chromium oxide is presented geometrically in Figure 7, and Figure 8 presents the measurement points in the interface area between the aluminum liquid phase and the chromium oxide substrate, obtained at the temperature of $1200\text{ }^\circ\text{C}$ and surrounding pressure P of 10^{-2} MPa. Values of the interfacial energy were calculated using the methodology proposed in [22] and are presented in Table 4. Results of the chemical composition measurement are shown in Table 5. Table 6 presents the results of quantitative chemical analysis of points #2 and #5 shown in Figure 8.

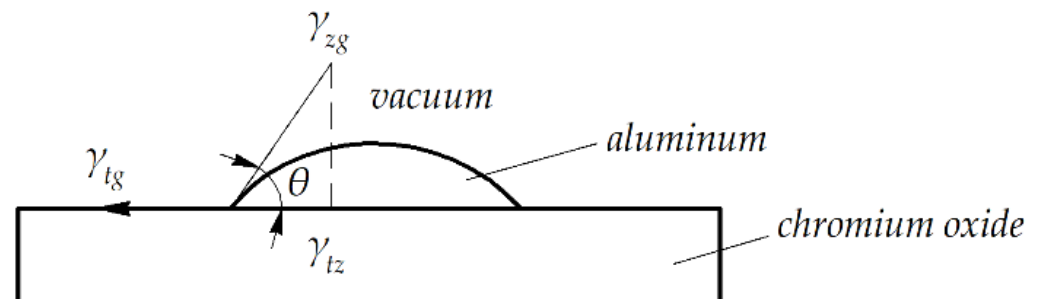


Figure 7. Geometrical representation of the equilibrium of liquid aluminum on the solid surface of chromium oxide.

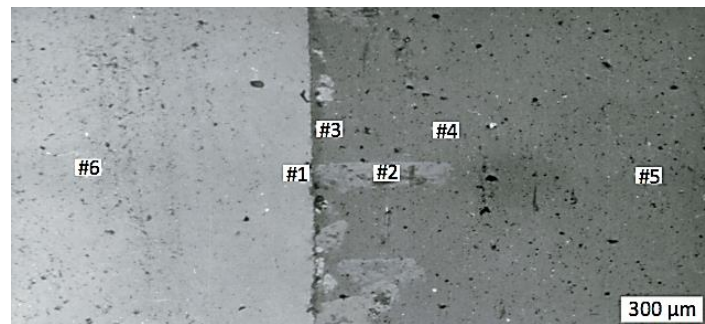


Figure 8. Interface between the aluminum droplet (brighter area on the left) and chromium oxide substrate (darker area on the right) obtained at $T = 1200\text{ }^{\circ}\text{C}$ and $P = 10^{-2}\text{ MPa}$. Numbers #1–#6 indicate places where chemical analysis was made.

Table 4. Contact angles and energy characteristics of the MeO–Me systems.

System	T , K	Adhesion Work W_a and Its Components, MJ/m^2				θ , $^{\circ}$	
		W_{ch}	W_b	Calculated	Experimental	Calculated	Experimental
$\text{Al}_2\text{O}_3\text{—Al}$	1500	510	243	753	1260 ± 50	98	60
$\text{Al}_2\text{O}_3\text{—Cr}$	2173	0	285	285	2260 ± 50	145	65
$\text{Cr}_2\text{O}_3\text{—Al}$	1573	730	235	955	1400 ± 50	118	60
$\text{Cr}_2\text{O}_3\text{—Cr}$	1573	605	260	865	1360 ± 50	120	65

Table 5. Content of chromium and aluminum at the respective points of MeO–Me interfaces.

Content, wt. %					
#1	#2	#3	#4	#5	#6
Cr/Al	Cr/Al	Cr/Al	Cr/Al	Cr/Al	Cr/Al
99.161/0.423	45.946/53.706	13.707/85.856	7.197/92.475	6.027/93.761	98.917/0.339

Table 6. Quantitative analysis of composition at the respective points of MeO–Me interfaces.

Content, wt. %					
#6			#5		
Cr	Al	O	Cr	Al	O
2.940	95.776	1.329	96.195	0.186	3.414

It should be noted from Table 4 that the work of adhesion in the system $\text{Cr}_2\text{O}_3/\text{Al}$ is higher than that of system $\text{Cr}_2\text{O}_3/\text{Cr}$. The contact angle in the $\text{Cr}_2\text{O}_3\text{—Al}$ system is smaller than that of $\text{Al}_2\text{O}_3\text{—Cr}$ or $\text{Cr}_2\text{O}_3\text{—Cr}$, both in calculations and in experiments. Chemical analysis (Table 5) suggests that in the phase interface, there is mutual diffusion of chromium and aluminum with prevailing activity of Cr. Thus, due to the good wettability of chromium oxide, the molten aluminum interacts with it during hot pressing, partially restoring chromium.

From Table 6 it can be seen that in the middle of the aluminum droplet (Figure 8), there is a small amount of oxygen, while the amount of diffusing chromium at point #2 was 2.940 wt.% against 0.186 wt.% aluminum at point #5 of the oxide substrate. This can be attributed to the diffusion process between chromium and aluminum ions.

The light observed phase consists of chromium, while the dark one consists of Cr, Al and O. At increased sintering temperatures, the content of aluminum in the dark phase increases, while that in the light phase decreases. Simultaneously, in the light phase, there is an increase in chromium content and decrease in oxygen content.

Microhardness measurement of the $\text{Cr}_2\text{O}_3 + (\text{Cr,Al})_2\text{O}_3 + \text{Cr}$ cermets demonstrated the dependence of microhardness on the restored chromium amount. This was expected

since other studies indicated an increase in Zn-Cr composite coating microhardness with increasing chromium content [37]. This might be the main explanation for the different microhardness values of dark and light phases, which were measured as $HV_d = 26 \pm 0.15$ GPa and $HV_l = 12 \pm 0.5$ GPa, respectively, under the load of 520 g. Moreover, the increased microhardness of chromium itself may be attributed to the additions of aluminum and iron since it is highly dependent on the technology and related additions and thus varies between $HV = 2$ and $HV = 10$ GPa [38]. Noteworthy, nanoindentation revealed the hardness of Cr_2O_3 thin films on SiO_2 glass substrate ranging from 12 to 22 GPa [39].

Figure 9 shows microstructure of $\text{Cr}_2\text{O}_3 + (\text{Cr,Al})_2\text{O}_3 + 22$ wt.% Cr cermet samples sintered at $T = 1500$ °C under $P = 30$ MPA for different lengths of time t . It can be seen that metallic chromium grains are distributed throughout the oxide matrix in the form of a number of clusters of small particles. This may be explained by the unsteady distribution of the liquid aluminum in the sample volume in the initial stage of the hot-pressing process.

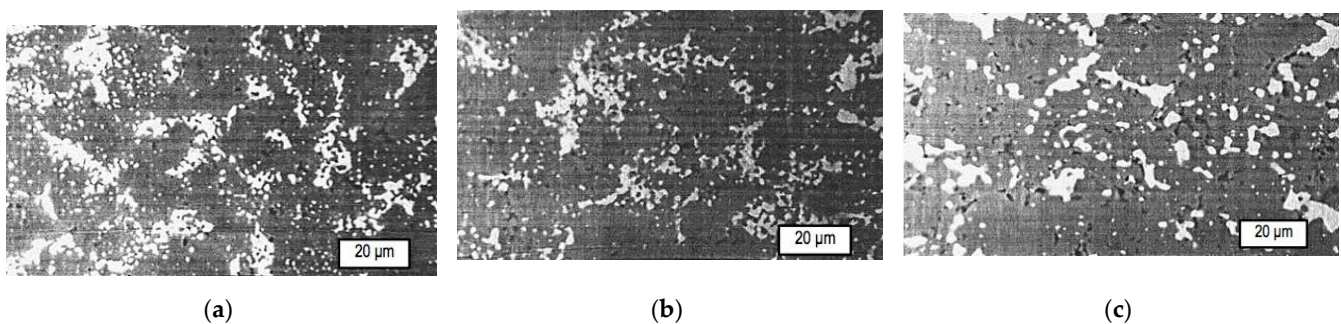


Figure 9. Microstructure of $\text{Cr}_2\text{O}_3 + (\text{Cr,Al})_2\text{O}_3 + 22$ wt.% Cr cermet samples sintered from $\text{Cr}_2\text{O}_3 + 13$ wt.% Al powder at $T = 1500$ °C under $P = 30$ MPA for different lengths of time t : (a) 5 min; (b) 10 min; (c) 15 min.

The composition of the solid solution $\text{Cr}_x\text{Al}_{2-x}\text{O}_3$ formed in the phase interfaces depends not only on the initial proportion, but also on the temperature and time of sintering. The dependence of the flexural strength σ_b on sintering temperature is plotted in Figure 10. It should be noted that eutectic proportion with 22 wt.% chromium (red curve #1) exhibited higher flexural strength than other proportions and than typical values for alumina ceramics, which range from 266.7 to 357.5 MPa [40]. The highest strength was obtained for the composition $\text{Cr}_2\text{O}_3 + (\text{Cr,Al})_2\text{O}_3 + 22$ wt.% Cr at $T = 1600$ °C after $t = 10$ min, perhaps as a result of the strongest bond between the phases that correspond with an equimolar composition of $(\text{Cr,Al})_2\text{O}_3$. The structure and fractogram of this cermet are presented in Figure 11.

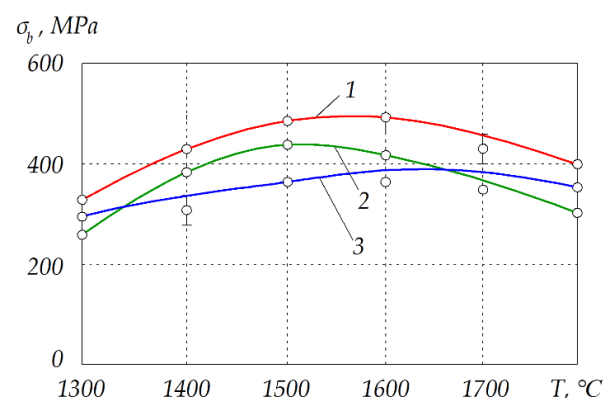


Figure 10. Dependence of flexural strength on sintering temperature of different cermets hot pressed under $P = 30$ MPA for $t = 10$ min: 1— $\text{Cr}_2\text{O}_3 + (\text{Cr,Al})_2\text{O}_3 + 22$ wt.% Cr; 2— $\text{Cr}_2\text{O}_3 + (\text{Cr,Al})_2\text{O}_3 + 30$ wt.% Cr; 3— $\text{Cr}_2\text{O}_3 + (\text{Cr,Al})_2\text{O}_3 + 15$ wt.% Cr.

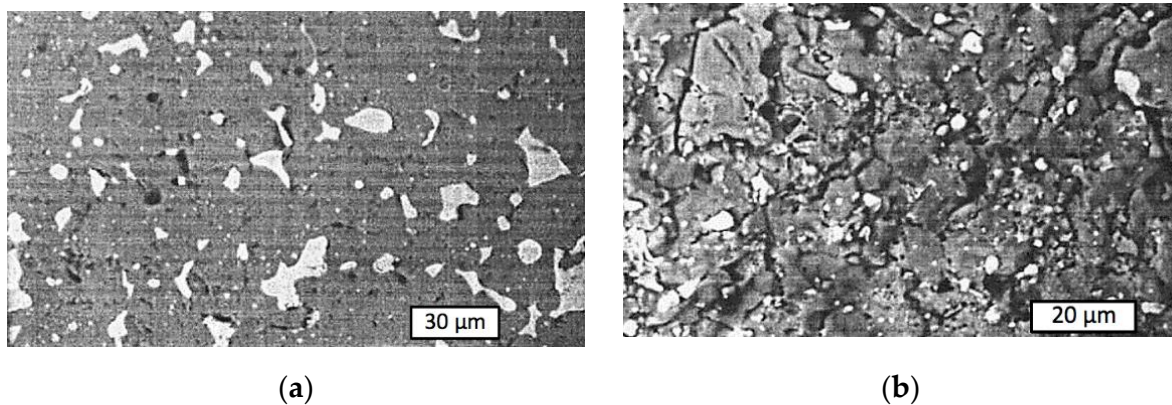


Figure 11. Cermet samples sintered from $\text{Cr}_2\text{O}_3 + 13 \text{ wt.}\% \text{ Al}$ powder at $T = 1600 \text{ }^\circ\text{C}$ under $P = 30 \text{ MPA}$ for $t = 10 \text{ min}$: (a) microstructure; (b) fractogram.

It can be assumed that the submicron dimensions of the grains seen in Figures 9 and 11 contributed to the improvement of the composite characteristics. As indicated by other studies, nanometric particles of materials, including Cr_2O_3 , usually provide physical and mechanical properties superior to those of conventional particles [41].

Fracture toughness results for different aluminum contents are presented graphically in Figure 12. The comparative analysis revealed that the highest value of K_{IC} can be obtained for the $\text{Cr}_2\text{O}_3 + 13 \text{ wt.}\% \text{ Al}$ proportion of the initial powders, which resulted in the desired $\text{Cr}_2\text{O}_3 + (\text{Cr,Al})_2\text{O}_3 + 22 \text{ wt.}\% \text{ Cr}$ composition of the cermet. Crack propagation in its structure is illustrated in Figure 13.

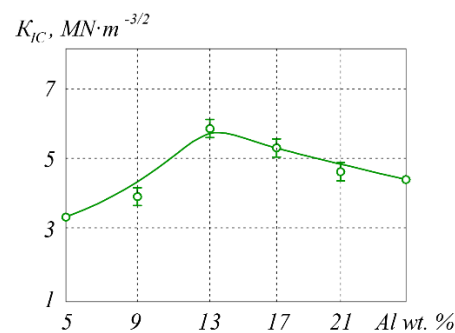


Figure 12. Fracture toughness of cermet samples sintered from initial powders of $\text{Cr}_2\text{O}_3 + \text{Al}$ with different proportions of aluminum at $T = 1600 \text{ }^\circ\text{C}$ under $P = 30 \text{ MPA}$ for $t = 10 \text{ min}$.

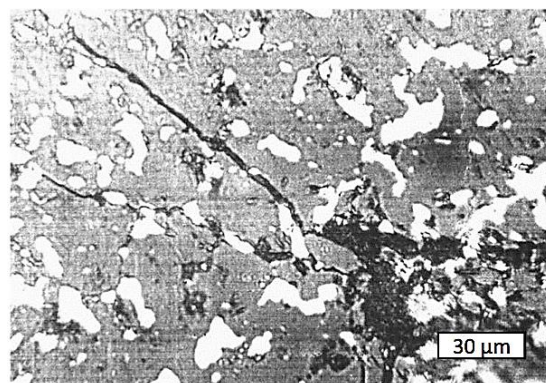


Figure 13. Crack propagation in the $\text{Cr}_2\text{O}_3 + (\text{Cr,Al})_2\text{O}_3 + 22 \text{ wt.}\% \text{ Cr}$ cermet sample sintered at $T = 1600 \text{ }^\circ\text{C}$ under $P = 30 \text{ MPA}$ for $t = 10 \text{ min}$.

From the microstructure seen in Figure 13, it can be concluded that the fracture toughness is increased due to the presence and dimensions of the grains of chromium in the matrix. The deflection of cracks bypassing the light phase grains obviously contributed to the toughening of the composite, while strong interface bonds determined its strength. This is consistent with other published studies indicating that weak interfaces are detrimental to composite strength and that the matrix carries a part of the load when the interfaces are strong [42]. Crack deflection is considered in toughening models [43] since it simply changes the value of K_{IC} compared to the case of straight crack propagation. The crack deflection mechanism is related to the changes in applied stress and its reduction in the crack front, which require high energies for cracks to achieve critical size [44].

5. Conclusions

The investigations in this study were focused on the hot-pressing process of chromia-based cermets. The ability of the sintering method to produce a eutectic composition of chromia and alumina was demonstrated through the mechanism of an aluminothermic reaction. The eutectic composition with 22 wt.% restored chromium was successfully sintered from a $\text{Cr}_2\text{O}_3 + 13$ wt.% Al initial powder mixture. During the reaction, chromium was restored, providing cermets of different chemical compositions. It was found that due to the presence of aluminum powder, full densification could be reached at 1600 °C after 2–3 min. On the other hand, the sintering in temperature interval between 1300 °C and 1400 °C under the pressure of 30 MPa would result in full completion of the restoration reaction and thus no pure aluminum content. It was found that during the hot pressing, aluminum melted, introducing a liquid phase to the sintered powders, which served as a sintering aid for the ceramic matrix composite.

Another important mechanism supporting the fabrication of the chromia-based composite was the appearance of the solid solution. Unlike the cermets obtained from mixtures of chromium and chromium oxide, the tested samples with added aluminum contained a solid solution of $(\text{Cr,Al})_2\text{O}_3$ in the interfaces between the phases after sintering. Solid solution $\text{Al}_{2-x}\text{Cr}_x\text{O}_3$ with varying stoichiometric composition had a strong effect on the boundaries between phases and thus on the overall mechanical strength of the composite. The tested cermets exhibited differentiation of properties, mainly determined by the metal and ceramic characteristics, the volume proportion between them and the adhesion energies, but also by the initial powders, their morphology (particle dimensions and shape) and sintering conditions. Sintering conditions have a direct impact on the stoichiometric composition of the solid solution in the phase interface which determines the mechanical properties of the cermet composite.

The highest strength and toughness were reached for the eutectic composition $\text{Cr}_2\text{O}_3 + (\text{Cr,Al})_2\text{O}_3 + 22$ wt.% Cr, where 22 wt.% was restored chromium. Sintered at $T = 1600$ °C under $P = 30$ MPa for $t = 10$ min, it exhibited flexural strength $\sigma_b = 490$ MPa and fracture toughness $K_{IC} = 5.8$ MN/m^{3/2}. These characteristics are advantageous for ceramic cutting tools, so this seems to be a promising research direction. Further investigations will provide comparative characteristics of the obtained cermet and typical alumina-based materials of cutting tools, as well as an analysis of the ways for further improvement.

Author Contributions: Conceptualization, E.G., V.N. and D.M.; methodology, E.G., W.Z., V.B. and V.N.; software, D.M. and K.K.; validation, M.R., L.C. and K.K.; formal analysis, W.Z., L.C., V.B. and E.G.; investigation, V.N., M.R. and D.M.; resources, D.M., V.B. and W.Z.; data curation, E.G. and K.K.; writing—original draft preparation, V.N.; writing—review and editing, M.R., V.B., W.Z. and D.M.; visualization, M.R. and K.K.; supervision, V.N.; project administration, E.G. and L.C.; funding acquisition, E.G. and L.C. All authors have read and agreed to the published version of the manuscript.

Funding: The article was prepared as part of a study under the state budget topic The Use of Non-traditional Methods of Obtaining Nanopowders and Sintering in the Development of Modified Mullite–ZrO₂ Ceramics Resistant to Heat Shock (State Registration Number 0121U109441) with the financial support of the Ministry of Education and Science of Ukraine, in connection with the Specific Research Projects SP2022/131 Specific research of production and measurement of complex shape surfaces and SP2022/50 Specific research of machining and 3D printing technologies financed by the Ministry of Education, Youth and Sports and Faculty of Mechanical Engineering VŠB-TUO.

Institutional Review Board Statement: Not applicable.

Informed Consent Statement: Not applicable.

Data Availability Statement: Data available on request due to privacy restrictions.

Conflicts of Interest: The authors declare no conflict of interest.

References

1. Eray, S. Application of metal oxides in composites. In *Metal Oxides*; Al-Douri, Y., Ed.; Elsevier: Amsterdam, The Netherlands, 2020; pp. 101–119. [\[CrossRef\]](#)
2. Wang, X.; Zhao, J.; Gan, Y.; Tang, X.; Gai, S.; Sun, X. Cutting performance and wear mechanisms of the graphene-reinforced Al₂O₃-WC-TiC composite ceramic tool in turning hardened 40Cr steel. *Ceram. Int.* **2022**, *48*, 13695–13705. [\[CrossRef\]](#)
3. Wang, X.; Zhao, J.; Cui, E.; Liu, H.; Dong, Y.; Sun, Z. Effects of sintering parameters on microstructure, graphene structure stability and mechanical properties of graphene reinforced Al₂O₃-based composite ceramic tool material. *Ceram. Int.* **2019**, *45 Part B*, 23384–23392. [\[CrossRef\]](#)
4. Gevorkyan, E.; Mamalis, A.; Vovk, R.; Semiatkowski, Z.; Morozow, D.; Nerubatskyi, V.; Morozova, O. Special features of manufacturing cutting inserts from nanocomposite material Al₂O₃-SiC. *J. Instrum.* **2021**, *16*, P10015. [\[CrossRef\]](#)
5. Hong, D.; Yin, Z.; Yan, S.; Xu, W. Fine grained Al₂O₃/SiC composite ceramic tool material prepared by two-step microwave sintering. *Ceram. Int.* **2019**, *45*, 11826–11832. [\[CrossRef\]](#)
6. Zhang, Z.; Liu, Y.; Liu, H. Mechanical properties and microstructure of spark plasma sintered Al₂O₃-SiCw-Si₃N₄ composite ceramic tool materials. *Ceram. Int.* **2022**, *48*, 5527–5534. [\[CrossRef\]](#)
7. Yin, Z.; Huang, C.; Zou, B.; Liu, H.; Zhu, H.; Wang, J. Dynamic fatigue behavior of Al₂O₃/TiC micro-nano-composite ceramic tool materials at ambient and high temperatures. *Mater. Sci. Eng. A* **2014**, *593*, 64–69. [\[CrossRef\]](#)
8. Wang, D.; Xue, C.; Cao, Y.; Zhao, J. Microstructure design and preparation of Al₂O₃/TiC/TiN micro-nano-composite ceramic tool materials based on properties prediction with finite element method. *Ceram. Int.* **2018**, *44*, 5093–5101. [\[CrossRef\]](#)
9. Gevorkyan, E.; Rucki, M.; Krzysiak, Z.; Chishkala, V.; Zurowski, W.; Kucharczyk, W.; Barsamyan, V.; Nerubatskyi, V.; Mazur, T.; Morozow, D.; et al. Analysis of the Electroconsolidation Process of Fine-Dispersed Structures Out of Hot Pressed Al₂O₃-WC Nanopowders. *Materials* **2021**, *14*, 6503. [\[CrossRef\]](#)
10. Oguntuyi, S.D.; Johnson, O.T.; Shongwe, M.B. Spark plasma sintering of ceramic matrix composite of TiC: Microstructure, densification, and mechanical properties: A review. *Int. J. Adv. Manuf. Technol.* **2021**, *116*, 69–82. [\[CrossRef\]](#)
11. Krenkel, W. *Ceramic Matrix Composites*; Wiley-VCH: Berlin, Germany, 2008.
12. Konopka, K. Particle-Reinforced Ceramic Matrix Composites—Selected Examples. *J. Compos. Sci.* **2022**, *6*, 178. [\[CrossRef\]](#)
13. Ding, H.; Bao, X.; Jamili-Shirvan, Z.; Jin, J.; Deng, L.; Yao, K.; Gong, P.; Wang, X. Enhancing strength-ductility synergy in an ex situ Zr-based metallic glass composite via nanocrystal formation within high-entropy alloy particles. *Mater. Des.* **2021**, *210*, 110108. [\[CrossRef\]](#)
14. Prokopiv, N.; Kharchenko, O.; Gevorkyan, E.; Gutsalenko, Y. Exploring the process to obtain a composite based on Cr₂O₃-AlN using a method of hot pressing. *East.-Eur. J. Enterp. Technol.* **2019**, *3*, 17–21. [\[CrossRef\]](#)
15. Xia, J.F.; Nian, H.Q.; Liu, W.; Wang, X.G.; Jiang, D.Y. Effect of Cr₂O₃ derived from Cr(NO₃)₃·9H₂O precursor on the densification and mechanical properties of zirconia-toughened alumina (ZTA) composites. *Ceram. Int.* **2016**, *42*, 9116–9124. [\[CrossRef\]](#)
16. Corberán, V.C.; Rives, V.; Stathopoulos, V. Recent Applications of Nanometal Oxide Catalysts in Oxidation Reactions. In *Advanced Nanomaterials for Catalysis and Energy*; Sadykov, V.A., Ed.; Elsevier: Amsterdam, The Netherlands, 2019; pp. 227–293. [\[CrossRef\]](#)
17. Ratia, V.L.; Zhang, D.; Daure, J.L.; Shipway, P.H.; McCartney, D.G.; Stewart, D.A. Sliding wear of a self-mated thermally sprayed chromium oxide coating in a simulated PWR water environment. *Wear* **2019**, *426–427 Pt B*, 1466–1473. [\[CrossRef\]](#)
18. Sun, H.; Yi, G.; Wan, S.; Kong, C.; Zhu, S.; Bai, L.; Yang, J. Effect of Cr₂O₃ addition on mechanical and tribological properties of atmospheric plasma-sprayed NiAl-Bi₂O₃ composite coatings. *Surf. Coat. Technol.* **2021**, *427*, 127818. [\[CrossRef\]](#)
19. Das, B.; Gopinath, M.; Nath, A.K.; Bandyopadhyay, P.P. Online monitoring of thermo cycles during laser remelting of flame sprayed chromia coating in pulsed mode and coating properties. *Optik* **2021**, *227*, 166030. [\[CrossRef\]](#)
20. Gerald, O.J.; Wenge, L.; Tao, Z.Y.; Long, L.C.; Qiang, L. Influence of plasma spraying current on the microstructural characteristics and tribological behaviour of plasma sprayed Cr₂O₃ coating. *Bol. Soc. Esp. Ceram. Vidr.* **2021**, *60*, 338–346. [\[CrossRef\]](#)
21. Rondinella, A.; Furlani, E.; Magnan, M.; Scagnetto, F.; Driussi, S.; Marin, E.; Maschio, S. Synthesis, crystallographic characterization, and mechanical behavior of alumina chromia alloys. *Ceram. Int.* **2021**, *47*, 24494–24500. [\[CrossRef\]](#)
22. Kisly, P.S.; Bodnaruk, N.I.; Borovikova, M.S. *Cermets*; Naukova Dumka: Kyiv, Ukraine, 1985. (In Russian)

23. Turkevich, V.Z.; Shishkin, B.A. High temperature calorimeter up to 2050 K. In Proceedings of the 9th National Conference on Thermal Analysis, Kyiv, Ukraine; 1985; p. 31.
24. Strizhalo, V.A.; Novogrudsky, L.S.; Vorobyov, E.V. *Strength of the Alloys for Cryogenic Devices under Electromagnetic Influence*; Naukova Dumka: Kyiv, Ukraine, 1990. (In Russian)
25. Gevorkyan, E.; Nerubatskyi, V.; Chyshkala, V.; Morozova, O. Revealing specific features of structure formation in composites based on nanopowders of synthesized zirconium dioxide. *East.-Eur. J. Enterp. Technol.* **2021**, *5*, 6–19. [[CrossRef](#)]
26. Gevorkyan, E.; Nerubatskyi, V.; Chyshkala, V.; Gutsalenko, Y.; Morozova, O. Determining the influence of ultra-dispersed aluminum nitride impurities on the structure and physical-mechanical properties of tool ceramics. *East.-Eur. J. Enterp. Technol.* **2021**, *6*, 40–52. [[CrossRef](#)]
27. Zhao, P.; Zhang, H.; Gao, H.; Zhu, Y.; Yu, J.; Fan, R.; Zhao, H. Formation process and properties of aluminium–chromium slag. *Ceram. Int.* **2018**, *44*, 15730–15734. [[CrossRef](#)]
28. Karapetyantz, M.H. *Introduction to the Chemical Processes Theory*; Higher School Press: Moscow, Russia, 1970.
29. Vlasov, A.O. Ceramic composite materials. *J. Sov. Chem. Soc.* **1982**, *27*, 50–56. (In Russian)
30. Nalepka, K.; Peçcherski, R.B. The strength of the interfacial bond in the ceramic matrix composites Al₂O₃-Ni. *Mech. Control* **2010**, *29*, 132–137.
31. Vuurman, M.A.; Wachs, I.E.; Stufkens, D.J.; Oskam, A. Characterization of chromium oxide supported on Al₂O₃, ZrO₂, TiO₂, and SiO₂ under dehydrated conditions. *J. Mol. Catal.* **1993**, *80*, 209–227. [[CrossRef](#)]
32. Fierro, J.L.G. *Metal Oxides: Chemistry and Applications*; CRC Press: Boca Raton, FL, USA, 2006.
33. Bansal, N.P. *Handbook of Ceramic Composites*; Kluwer Academic Publishers: New York, NY, USA, 2005.
34. Comyn, J. What are adhesives and sealants and how do they work? In *Adhesive Bonding*, 2nd ed.; Adams, R.D., Ed.; Woodhead Publishing: Cambridge, MA, USA, 2021; pp. 41–78. [[CrossRef](#)]
35. Brogly, M. Forces Involved in Adhesion. In *Handbook of Adhesion Technology*; da Silva, L., Öchsner, A., Adams, R., Eds.; Springer: Cham, Switzerland, 2018; pp. 43–70. [[CrossRef](#)]
36. Leite, F.L.; Bueno, C.C.; Da Róz, A.L.; Ziemath, E.C.; Oliveira, O.N. Theoretical Models for Surface Forces and Adhesion and Their Measurement Using Atomic Force Microscopy. *Int. J. Mol. Sci.* **2012**, *13*, 12773–12856. [[CrossRef](#)] [[PubMed](#)]
37. Tahraoui, L.; Diafi, M.; Aidi, A.; Benhaoua, B. Chromium-rich Zn–Cr alloys: Electrochemical deposition, structure and corrosion resistance. *Dig. J. Nanomater. Biostruct.* **2021**, *16*, 191–196.
38. Anger, G.; Halstenberg, J.; Hochgeschwender, K.; Scherhag, C.; Korallus, U.; Knopf, H.; Schmidt, P.; Ohlinger, M. Chromium Compounds. In *Ullmann's Encyclopedia of Industrial Chemistry*; Wiley-VCH: Berlin, Germany, 2005. [[CrossRef](#)]
39. Jõgiaas, T.; Tarre, A.; Mändar, H.; Kozlova, J.; Tamm, A. Nanoindentation of Chromium Oxide Possessing Superior Hardness among Atomic-Layer-Deposited Oxides. *Nanomaterials* **2022**, *12*, 82. [[CrossRef](#)]
40. Ćurković, L.; Bakić, A.; Kodvanj, J.; Haramina, T. Flexural strength of alumina ceramics: Weibull analysis. *Trans. FAMENA* **2010**, *34*, 13–19.
41. Gómez-Rodríguez, C.; Antonio-Zárate, Y.; Revuelta-Acosta, J.; Verdeja, L.F.; Fernández-González, D.; López-Perales, J.F.; Rodríguez-Castellanos, E.A.; García-Quiñonez, L.V.; Castillo-Rodríguez, G.A. Research and Development of Novel Refractory of MgO Doped with ZrO₂ Nanoparticles for Copper Slag Resistance. *Materials* **2021**, *14*, 2277. [[CrossRef](#)]
42. Lamon, J. Properties and Characteristics of SiC and SiC/SiC Composites. In *Comprehensive Nuclear Materials*, 2nd ed.; Konings, R.J.M., Stoller, R.E., Eds.; Elsevier: Amsterdam, The Netherlands, 2020; pp. 400–418. [[CrossRef](#)]
43. Ovid'ko, I.A.; Sheinerman, A.G. Toughening due to crack deflection in ceramic- and metal-graphene nanocomposites. *Rev. Adv. Mater. Sci.* **2015**, *43*, 52–60.
44. Luiz, A.F.; Tomaz, Í.V.; Oliveira, M.P.; Simão, L.; Monteiro, S.N. Development and evaluation of TiB₂-AlN ceramic composites sintered by spark plasma. *Ceram. Int.* **2016**, *42*, 18718–18723. [[CrossRef](#)]